RSC Advances

ROYAL SOCIETY OF CHEMISTRY

www.rsc.org/advances

Table of Contents

Y. El Mendili[1*], B. Minisini[2], A. Abdelouas[1] and J.-F. Bardeau[3]

RSC Advances., 2014, **XX**, YY.

We report on the first assignment of the Raman-active vibrational modes of mackinawite using Density Functional Perturbation Theory and direct method with BLYP + dispersion correction. Based on experimental data and calculation results, the Raman bands were assigned as 236 cm^{-1} (B_{1g}), 256 cm^{-1} (E_g), 376 cm^{-1} (A_{1g}) and 395 cm^{-1} (E_g).

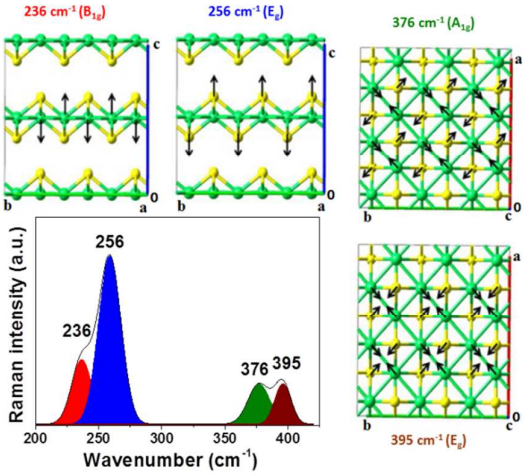

Assignment of Raman-active vibrational modes of tetragonal mackinawite: Raman investigations and Ab-Initio Calculations

Y. El Mendili[1*], B. Minisini[2], A. Abdelouas[1], J.-F. Bardeau[3]

[1] SUBATECH, CNRS-IN2P3, Ecole des Mines de Nantes, Université de Nantes, 4 rue Alfred Kastler, BP 20722, 44307 Nantes cedex 03, France

[2] ISMANS, 44 Avenue F A Bartholdi, 72000, Le Mans, France.

[3] LUNAM Université, Institut des Molécules et Matériaux du Mans, UMR CNRS 6283, Université du Maine, Avenue Olivier Messiaen, 72085 Le Mans Cedex 9, France

*Corresponding authors.

(Y. El Mendili) : E-mail: elmendil@subatech.in2p3.fr

Phone: 33-2 51 85 86 35; Fax: 33-2 51 85 84 52

Abstract

Mackinawite mineral was prepared as a carbon steel corrosion product in sulfidogenic waters at 90°C after 2 months. The tetragonal crystal structure of the material was confirmed by Rietveld refinement of X-ray diffraction (XRD) data, and vibrational modes were analysed by micro-Raman spectroscopy. Despite a large number of studies on the formation and the stability of tetragonal mackinawite, the interpretation of the Raman spectra remains uncertain. In the present study, we report on the first calculation of the Raman-active vibrational modes of mackinawite using Density Functional Perturbation Theory and direct method with BLYP + dispersion correction. Based on the comparison between calculated and experimental results, the four fundamental vibrational modes were assigned as 228 cm^{-1} (B_{1g}), 246 cm^{-1} (E_g), 373 cm^{-1} (A_{1g}) and 402 cm^{-1} (E_g).

1. Introduction

The mackinawite was first discovered by Evans et al.[1,2] from Mackinaw mine in Snohomish County, Washington, USA. It plays a critical role in serving as a precursor to the formation of most other stable iron sulfide phases[3-5] among which pyrite (FeS_2) is the most abundant[6]. Mackinawite (FeS) which forms naturally in recent sediments,[6] in active hydrothermal systems on or near the mid-ocean ridges,[7] can be produced via certain bacteria[8] and in particular the sulfate reducing bacteria (SRB)[9-12]. Mackinawite is also considered to be the first iron sulfide phase to form in most ambient environments and anoxic marine sediment[13].

In recent studies, it was reported that mackinawite has an ability to immobilize heavy metal atoms through sorption mechanisms[7, 14-20]. Mackinawite may also immobilize pollutant metals such as chromium[21] and selenium[22] through abiotic reduction thus playing an important role in the remediation of contaminated sites. In addition, mackinawite is an excellent material that was proposed to sorb mercury for marine environment[23-26].

In literature, though the vibrational spectra of mackinawite have been the subject of many investigations for years, several ambiguities and contradictions remain present in literature for the vibrational attribution[27-35]. The principal difficulty found in the natural environment, is the coexistence of porous iron sulfide and various structural mackinawite phases, as shown in our previous studies[5,12]. In addition, mackinawite-like phases are very sensitive towards oxidation which can also occur during transport and sample's preparation[12,32]. In order to overcome these problems, it is necessary to synthesis a crystalline mackinawite.

The synthesis of tetragonal mackinawite was first reported by Berner,[36,37] by immersing reagent grade metallic iron wire in a aqueous solution saturated with H_2S. Three main schemes describing the mechanisms of mackinawite formation have been reported[38-44]: the reaction of aqueous S(–II) solutions with either (i) metallic iron Fe(0) or (ii) a ferrous solution Fe(+II), and (iii) via using sulfate-reducing bacteria. In general, the first method leads to a crystalline mackinawite phase with a stoichiometric composition,[38,39] whereas the other processes form preferentially disordered mackinawite[40,41] or disordered mackinawite-like phases[42-44].

Recently, we reported on a method to form a mackinawite layer as a steel corrosion product[45]. The formation of pure tetragonal mackinawite was confirmed by X-Ray Diffraction (XRD) analysis after immersion of steel coupons in a Na_2S solution for 1 month at 30°C. In the study

conducted at 90°C,[5] with steel coupons immersed in Na_2S solutions, Raman investigations revealed clearly the formation of an initial phase attributed to poorly crystallized ferrous sulphide[54] followed by the formation of mackinawite. Micro-Raman spectroscopy was shown to be an effective and non-destructive technique for investigating the molecular structure of iron sulfides. Moreover, apart from its non-destructive character, there is a limited need of sample preparation and micro-Raman spectroscopy can provide detailed and specific information at a molecular level on the structure of molecules, thin films, with a high spatial resolution[47-50]. Regarding the ambiguities and contradictions present in the vibrational attribution of mackinawite in the literature, the analysis of the experimental Raman spectra and the assignment of the vibrational modes cannot be made satisfactorily without the additional support of theoretical calculations. Literature survey reveals that to the best of our knowledge, no theoretical studies, either quantum mechanical calculations on the mackinawite have been reported so far to examine and propose vibrational assignments.

Density Functional Theory (DFT) was successfully used for the characterization of electronic structure, magnetism, phonons and superconductivity of FeS, FeSe and FeTe compounds[51-56]. Devey et al.[51] from PAW calculation with PW91 functional, evaluated the influence of the Hubbard parameter on the stability and the electronic density of states of different FeS models to conclude that mackinawite is a nonmagnetic material whereas the incorporation of the Hubbard parameter lead to unphysical results. On the contrary, Kwon et al.,[52] using ultrasoft pseudopotential, treating both 3s and 3p states, in the valence in association with the PBE functional concluded that the ground state of mackninawite is single-stripe antiferromagnetic and that the DFT calculations cannot catch the real physic of FeS due to strong itinerant spin fluctuations. DFT calculations were also used to determine the lattice dynamics of isostructural compounds such as FeSe or FeTe. From Density Functional Perturbation Theory (DFPT) using ultra-soft pseudopotentials with LDA functional, Kumar et al.[53] concluded to the existence of a strong spin-phonon coupling in FeSe from phonon frequencies calculated. Always for FeSe, Gnezdilov et al.[54] observed a large hardening of the B_{1g}(Fe) phonon mode linked to the local fluctuations of the iron spin state from their calculations performed with a frozen phonon approach where all electron full potential linearized augmented plane wave was applied with LDA and PBEsol functionals. However, for FeTe, using non magnetic state with experimental cell parameters, Xia et al.[55] found a good agreement between the experimental B_{1g} mode frequency and the calculated one in the framework of the DFPT using ultra soft pseudopotentials with PBE functional. Their results

were confirmed by Okazaki et al.[56] after they compared A_{1g} and B_{1g} calculated frequencies with those measured for $Fe_{1.074}Te$.

In this study, we prepared a mackinawite layer as a steel corrosion product under sulfidogenic environment (Na_2S) at 90°C. The formation of pure tetragonal mackinawite was confirmed by X-Ray Diffraction (XRD) analysis and Raman spectra were recorded. The Raman-active vibrational modes of mackinawite were calculated using first-principle calculations and the DFT results were compared with experimental results in order to interpret and propose vibrational assignments

2. Experimental

2.1 Materials

The steel used in this study is P235GH, a heat-resistant pressure-vessel steel characterized by a good weldability. It is used above all for manufacturing boilers, pressure vessel and pipes transporting hot liquids. As already mentioned in our previous works,[5,12,45] the analysis were done on coupons machined into 10 × 10 × 1 mm, polished down to a surface roughness of 3 microns with a Buehler polisher and cleaned in a HCl (15%) + $NaCO_3$ (5%) solution as described in the ASTM standard method for corrosion measurement[57].

2.2 Mackinawite formation

Mackinawite being extremely sensitive to oxygen, all experiments have been done under strictly anaerobic conditions.

The steel coupons were placed in 100 ml sulfide-containing water[5]. Batch experiments were conducted at 90°C for 2 months in sulfide concentration of 1 mg/l. Anaerobic conditions were achieved first by degassing the medium using a vacuum pump and bubbling with 5% H_2/N_2 gas (2 bars).

2.3 X-ray Diffraction Analysis

X-ray diffraction (XRD) was first used to confirm the presence of mackinawite after 2 months of experiments. XRD pattern was recorded at room temperature using a Siemens D500 diffractometer in a Bragg- Brentano geometry using Cu-Kα_1 radiations (λ_1 = 1.5406) as X-ray source (cold cathode Crookes tube). This latter is generated by a 2200 W copper anode (from Siemens, KFL CU 2K model, maximum potential: 60 kV). The data were collected in the range 10° to 75° in 2θ with a 0.01° 2θ -step and a count time of 50s per step. The refinement

of the XRD data has been done using the JAVA based software namely Materials Analysis Using Diffraction (MAUD program).

2.4 Raman analysis

The iron sulfide phases formed on the steel surface were successfully identified using confocal micro-Raman analysis. The Raman spectra were recorded at room temperature in the back-scattering configuration on a T64000 Jobin-Yvon (Horiba) spectrometer under a microscope with a 100x objective focusing the 514 nm line from an Argon–Krypton ion laser (coherent, Innova). The Raman back-scattered light was filtered by a dielectric edge filter and analyzed by a spectrometer with a single monochromator (600 gratings mm^{-1}) coupled to a nitrogen cooled CCD detector. Using the 100x objective, the spot size of the laser is estimated to 0.8 μm and a very strong focused laser can easily reach power densities of a few mW/cm^2 within the focal spot. Therefore, for minimizing the possibility of degradation of the samples and phase modification under laser irradiation,[58,59] measurements were carried out with laser output powers between 1mW and 5 mW. The Raman spectra were systematically recorded twice in the wavenumber 100-2200 cm^{-1} region with an integration time of 360 s using the Labspec® software v.3.01 (Jobin Yvon-Horiba). As the baseline of the spectra are not perfectly flat, a standard polynomial background-subtraction postprocessing were systematically made using OriginPro 8.6 software version (OriginLab Corporation, Northampton, USA) before data analysis and curve-fitting procedures.

In the experiment section, we will present the Raman spectra only in the wavenumber regions 150-450 cm^{-1}.

It should be noted that the coupons were transported in a container under Argon gas before being analyzed by confocal micro-Raman spectroscopy to protect them from atmospheric contamination.

3. Results and discussion

3.1 X-ray Diffraction Analysis (XRD)

X-ray diffraction was used to confirm the presence of mackinawite after 2 months of experiments. The X-ray diffractogram of corroded steel (Fig. 1) shows the presence of a polycrystalline mackinawite phase (JCPDS 24-0073) since the positions, the line intensities and the narrowness of the peaks are in good agreement with previously reported data for

crystalline mackinawite (P4/nmm space group)[38,60]. Unit cell parameters derived from the diffraction pattern are a= b= 0.366 nm and c= 0.502 nm[46]. The observation of the less intense and broad peaks at about 26° and 46° indicates probably the presence of iron oxide due to the slight oxidation of steel surface during the XRD analysis. The refined average grain size values characteristics of the mackinawite phase are evaluated to 96 ± 5 nm.

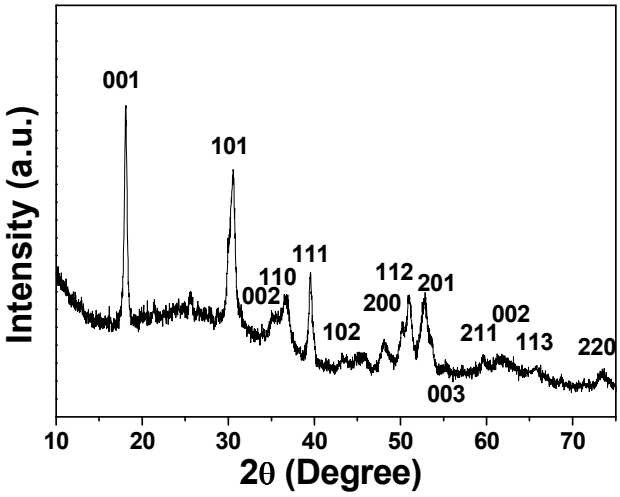

Fig. 1 XRD patterns of the steel corrosion products after exposition to sulfide concentrations of 1 mg/l for 2 months at 90°C.

3.2 Experimental Raman spectra

The Raman spectrum obtained on the steel surface after 15 days of immersion in Na_2S solution (Fig. 2-a) shows the presence of two bands around 285 and 210 cm^{-1} (bandwidths of 13 and 12 cm^{-1}, respectively). These bands have previously been attributed to the symmetric stretching mode and to a lattice mode of a poorly crystallized or amorphous FeS material[46]. These two bands were actually observed by Hansson et al.[46] during an anodic polarisation of an iron electrode in carbonated media. Using *in situ* micro-Raman spectroscopy, they detected these bands just after an immersion time of 5 min in a Na_2S solution. They assumed that these two vibrational bands corresponded to amorphous FeS, as already reported by Boughriet et al.[62] in anoxic sediments. Indeed, iron sulfides can be formed by the precipitation of Fe(II) and S(-II) in solutions and the initial precipitate was formerly designated as 'amorphous FeS'[63] or 'poorly ordered or disordered FeS'[46]. However, despite a large number of studies on the formation and phase transitions of iron sulfides, the exact structure and the physical properties of the first precipitate are not satisfactorily known. Lennie and Vaughan[64] showed

that this initial phase, which is sometimes referred to as "amorphous FeS," displays long-range mackinawite ordering. Recently, on the basis of low-angle X-ray powder diffraction analyses[42,59] and high resolution transmission electron microscopic study[65], it was demonstrated that this initial phase was made of nanocrystalline materials.

After 1 month of experiment, the corresponding Raman spectrum (Fig. 2-b) shows the presence of six bands around 210, 236, 258, 286, 376 and 395 cm^{-1}. This spectrum is similar to that reported by Bourdoiseau et al.,[27] but no Raman band assignment was given by these authors. As the Raman spectrum shows the presence of the modes at 210 and 286 cm^{-1} (with bandwidths of 9 and 12 cm^{-1}, respectively), it is reasonable to assume that these bands are characteristic of the initial iron sulfide product. The appearance of bands at 236, 258, 376 and 395 cm^{-1} (with bandwidths of 17, 16, 43 and 22 cm^{-1}, respectively) may suggest the coexistence of the initial phase with the crystalline mackinawite phase[5].

The Raman spectrum obtained on the steel surface after 2 months of immersion in Na_2S solution is presented in Fig. 2-c. The Raman active modes of the initial phase disappear from the spectrum and four well-defined vibrational modes at 228, 246, 373 and 402 cm^{-1} (with bandwidths of 16, 14, 38 and 15 cm^{-1}, respectively) are observed. According to the XRD results (Fig. 1), the four vibrational bands can be undoubtedly assigned to polycrystalline mackinawite.

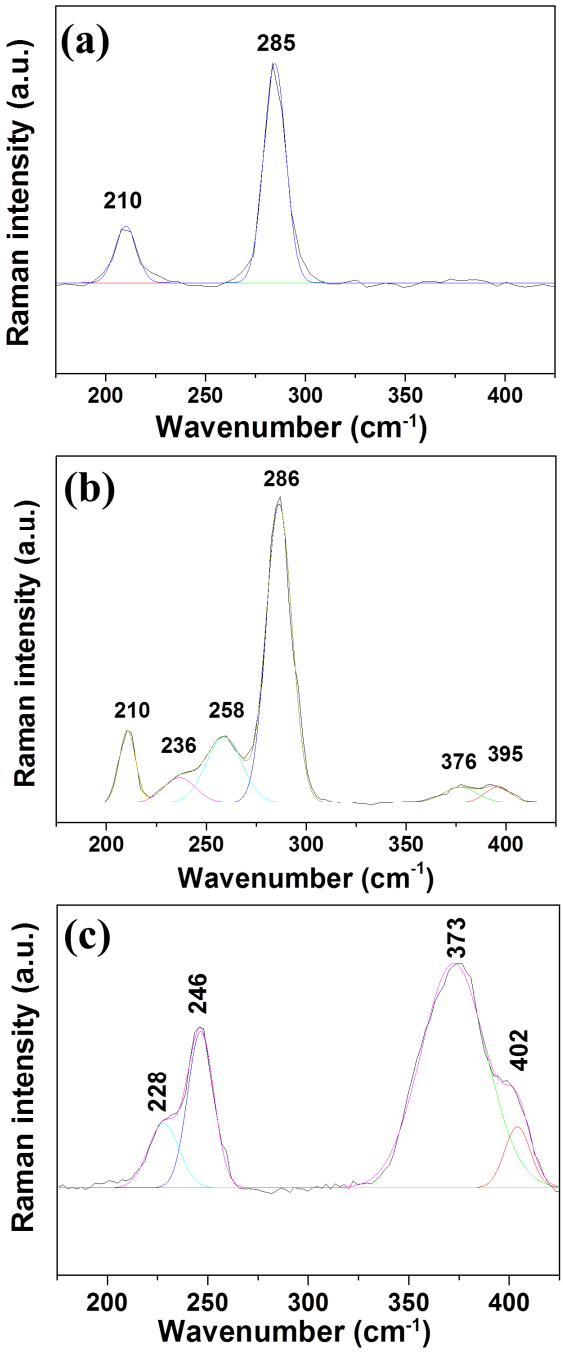

Fig. 2 Raman spectrum of steel coupons corroded under anaerobic conditions in presence of sulfide ions (1 mg/l), (a): after 15 days (b): after 1 month and (c): after 2 months of time experiment with curve fitting results.

As previously mentioned, several ambiguities and contradictions have been reported in the literature for the vibrational attribution of mackinawite modes. In the following, we give an overview of the most significant works on the experimental Raman characterization of mackinawite. According to Bourdoiseau et al.,[27,30] mackinawite (FeS) can present three physico-chemical states according to crystallization and oxidation: nanocrystalline

mackinawite, well-crystallized mackinawite and partially oxidized mackinawite, that is mackinawite containing some Fe(III) cations in its structure. Each of them leads to a characteristic Raman spectrum. According to these authors, nanocrystalline mackinawite was characterized by the presence of two sharp lines, at 208 and 282 cm^{-1} and the well-crystallised stoichiometric Fe(II)-mackinawite by three bands at 208, 256 and 298 cm^{-1}, [27] resulting from the crystallisation of the initial nanocrystalline mackinawite particles[28]. The presence of the mode at 208 cm^{-1} both in the Raman spectra of these two types of structure was not discussed, leaving many important questions unanswered and especially the relations between the so-called nanocrystalline mackinawite phase and the crystalline mackinawite phase; during a progressive crystallization the vibration modes should be shifted toward higher wavenumber. In addition, the Fe(III)-containing mackinawite was characterized by an intense doublet of peaks at 310-320 cm^{-1}, an intense peak at 248 cm^{-1} and an additional weak peak at 355 cm^{-1}, that may be attributed to the stretching modes of Fe(III)-S tetrahedrons according to these authors. The intense doublet of peaks at 310–320 cm^{-1} and the smaller peak at 355 cm^{-1} observed by Bourdoiseau et al. [27] were attributed to the vibration mode of partially oxidized mackinawite ($Fe^{II}_{1-3x}Fe^{III}_{2x}S$). The vibration mode at 355 cm^{-1} can also be attributed to the vibration of Greigite, which can form by the oxidation of mackinawite[30]. Greigite with formula Fe_3S_4 (Iron (II, III) sulfide), is the sulfur equivalent of the iron oxide magnetite (Fe_3O_4). It can be found in sediments and low-temperature hydrothermal deposits[66] and formed by magnetotactic bacteria and Sulphate reducing bacteria[67,68]. Greigite seems to form only from a FeS precursor[37,41,61,69] through an oxidation process of Fe(II) into Fe(III). For instance, dry oxidation of mackinawite exposed to air leads to greigite and ultimately to elemental sulfur, and magnetite[69].

Csákberényi-Malasics et al.[70] prepared iron sulfide using a procedure described by Chen et al. [71], in which $FeSO_4.7H_2O$ was mixed with thioacetamide solution (C_2H_5NS). The XRD analysis of iron sulfide precipitated showed the formation of a mixture of mackinawite and greigite. The XRD pattern shows also the presence of minor amounts of goethite due to the oxidation during sample transfer and aerobic XRD analyses. This result confirms those of Benning et al.[41] which, show that the freshly iron monosulfide precipitates are extremely sensitive to oxygen.

It should be noted that in our case the steel coupons were prepared under anaerobic conditions and were systematically transported in a container after immersion experiments and before being analyzed by confocal micro-Raman spectroscopy (in order to protect them

from atmospheric contamination and oxidation). Hence, the absence of the vibration mode attributed to the Fe(III)-containing mackinawite and greigite in our Raman spectra is likely due to a limited sample oxidation in air during the synthesis or before Raman analysis. This oxidation problem faced by many research teams is probably why to this day there is still no reference Raman spectrum of mackinawite.

In conclusion, our Raman investigations show the formation of an initial phase after the 15th days of experiment followed by the formation of mackinawite after 2 month. But, given the ambiguities and the contradictions present in the vibrational attribution of mackinawite, these experimental results are compared with DFT calculations.

4. Computational details

Based on the structural results reported by Lennie et al.[38] for FeS (P4/nmm, Z=2, a=3.67 Å, c= 5.03 Å), we performed full relaxation calculations with VASP 5.2[72] code as implemented within MEDEA Interface[73]. The generalized gradient approximation (GGA) through Becke-Lee-Yang-Parr (BLYP)[74,75] functional and projector augmented wave (PAW) were employed and the dispersive interactions were taken into account using the method proposed by Grimme[76] (as implemented in VASP 5.2). We run non magnetic calculations with a basis set of plane waves truncated at a kinetic energy of 500 eV. Brillouin zone integrations were performed by using a 9X9X7 k–points Monkorst-Pack grid for the optimization calculation[77]. The electronic iterations convergence was set at 10^{-5} eV whereas the convergence condition for the ionic relaxation loop was fixed at $2*10^{-2}$ eV/Å. The first order Methfessel-Paxton smearing with a width of 0.2 eV was used. The zone center phonon frequencies were evaluated from DFPT on the optimized structure whereas the complete phonon spectrum was obtained with PHONON code,[78] a direct method based on the harmonic approximation, as implemented in MEDEA with the forces evaluated by VASP 5.2. A 2X2X2 supercell consisting of 36 atoms was generated from the previously optimized cell.

The unit cell of mackinawite FeS contains 4 atoms in the P4/nmm (D^7_{4h}) structure; hence, it supports 3 X 4 = 12 modes of vibration, out of which three are acoustic and the remaining 9 modes are optical modes at **q**=0, defined as G or Γ point in reciprocal space.

The symmetry of the modes is related to the symmetry of the crystal structure by the character table obtained from group theoretical analysis. The character table for the point group D^7_{4h} (4/nmm) is given in Table 1.

Table 1 : Character table of the point group D^7_{4h} (4/nmm) from Bilbao crystallographic server[79], international (Hermann-Mauguin) notation is used to defined the symmetry element

D^7_{4h} (4/nmm)	1	2	4	2_h	$2_{h'}$	-1	m_z	-4	m_v	m_d	functions
Multiplicity	1	1	2	2	2	1	1	2	2	2	
A_{1g}	1	1	1	1	1	1	1	1	1	1	x^2+y^2,z^2
A_{2g}	1	1	1	-1	-1	1	1	1	-1	-1	J_Z
B_{1g}	1	1	-1	1	-1		1	-1	1	-1	x^2-y^2
B_{2g}	1	1	-1	-1	1	1	1	-1	-1	1	xy
E_g	2	-2	0	0	0	2	-2	0	0	0	(xz,yz),(J_x, J_y)
A_{1u}	1	1	1	1	1	-1	-1	-1	-1	-1	
A_{2u}	1	1	1	-1	-1	-1	-1	-1	1	1	z
B_{1u}	1	1	-1	1	-1	-1	-1	1	-1	1	
B_{2u}	1	1	-1	-1	1	-1	-1	1	1	-1	
E_u	2	-2	0	0	0	-2	2	0	0	0	(x,y)

The selection rules associated to the positions of the two independent atoms in the primitive cell situated in Wickoff positions 2a and 2c lead to the following irreducible representation.

$$\Gamma: 2E_u \oplus 2A_{2u} \oplus B_{1g} \oplus 2E_g \oplus A_{1g}$$

In this analysis, the A_{2u} and E_u modes are infrared active and the A_{1g}, B_{1g}, E_g modes are Raman active.

4.1 Theoretical study

The optimized parameters are *a* = 3.61 Å and *c* = 4.95 Å leading to a *c/a* ratio of 1.371. These results lead to a discrepancy inferior to 1.5% comparatively to experimental results. It is worth noting to underline the effect of taking into account the Van der Waals interactions in the formalism of Grimm, since the *c* parameter, calculated with BLYP alone, overestimated the experimental value of 25% with a value of 6.32 Å whereas the parameter *a* remained relatively constant at 3.67 Å. However, as observed by Kwon et al.[72] with ultra-soft pseudopotential associated to PBE functional, the *z* coordinate of Sulfur along the *c* axis differs by 5%, 0.247 for the calculated value against 0.26 for the experimental crystal cell. This value was better predicted for the single stripe antiferromagnetic structure but to the detriment of the Fe-Fe bond length since the discrepancy with experimental results was then of 4.31%. Moreover, the measurements were performed at room temperature where the antiferromagnetic state is unstable. Consequently, we performed the frequencies calculation using a non magnetic structure.

Solving the equation of motion for a 3D crystal provides some eigenvalues (ω, the pulsation) associated to eigenvectors (atomic displacement vectors) depending on a wave vector of propagation given as a vector (**q**) in reciprocal space. Dispersion relation is therefore define as ω=ω(**q**). The directions of the wave vectors of general interest are defined by the points of high symmetry of the irreducible Brillouin zone. The **q** vector types of space group P4/nmm can be found elsewhere.[80]

The phonon dispersion curves along several lines of high symmetry for the FeS structure optimized at 0K and 0 MPa are shown in Fig. 3. No negative frequencies are present indicating that the structure is dynamically stable. Each full line represents ω=ω(**q**) for a given direction, for example **GM** for the left part. Three acoustic modes, active at low energy (low pulsation), are linked to in phase atomic displacements. The degenerate modes at G point, split into three branches following the directions **GM** and **GX** and two branches following **GZ**. One branch defined as transverse is associated to atomic modulations orthogonal to wave. Atomic modulation is parallel to wave vector for the two others branches, which can be degenerated, and are said longitudinal At higher energy are found the 3N-3 optical modes linked to out of phase atomic movements. In the Table 2 are given the frequencies of active phonon calculated from DFPT, direct method and the experimental values.

Table 2 : DFPT and direct method calculated and experimental frequencies in units of cm^{-1}. The degeneracy of the modes is given after the slash symbol. Assigned Raman active modes are given in bold whereas the Infra Red active modes are given in italic

DFPT	**Direct Method**	**Experimental Data**
248 / 1	225 / 1 (**B_{1g}**)	228
247 / 2	243 / 2 (**E_g**)	246
372 / 2	372 / 2 (*E_u*)	
390 / 1	388 / 1 (**A_{1g}**)	373
392 / 1	396 / 1 (*A_{2u}*)	
395 / 2	396 / 2 (**E_g**)	402

The major discrepancy concerning the calculated values is observed for the non degenerated mode calculated at 248 cm^{-1} and 225 cm^{-1} by DFPT and direct method respectively. By symmetry analysis this mode was assigned to the B_{1g} mode and can be matched to the experimental value measured at 228 cm^{-1}. The frequency of the B_{1g} mode, attributed to the translation of the iron atoms in the direction of the c-axis, was overestimated by 6 to 18 % for FeSe[54] and by 10 to 40 % for FeTe[55] in function of the experimental temperature and the magnetic state or the cell parameters of the crystal models. On another way, the frequency of this mode remained relatively constant for FeSe and FeTe since it was experimentally measured at 202 and 206.5 cm^{-1} for $Fe_{1.074}Te$ at 5 K and FeSe at 7K respectively. In presence of sulfur, this mode is expected to shift by more than 20 cm^{-1} on the base of the anharmonicity effect observed for FeSe[54]. By increasing the temperature from 7 K to 295 K, the frequency of the B_{1g} mode drop from 206.5 to 193.9 cm^{-1}. The E_g mode calculated at 243 cm^{-1} (248 cm^{-1} by DFPT) can be assigned to an out-of-phase radial translation of the iron and sulfur atoms in the direction $[1\ \ 1\ \ 0]$ and $[\bar{1}\ \ 1\ \ 0]$, respectively, leading to an angular distortion of the FeS_4 tetrahedra. This mode is the softnest for FeSe[54] and FeTe[55] with a calculated value for a non magnetic relaxed cell of 143 and 73.3 cm^{-1} respectively. Concerning the A_{1g} mode implying the translation of the sulfur atoms parallel to the *c*-axis the calculated value was 388 cm^{-1} (390 cm^{-1} by DFPT) and could be attributed to the experimental value of 373 cm^{-1}. A such overestimation was also noticed for FeSe[54] and FeTe,[55] mainly for the phonon calculations performed on the relaxed structures. As for Eg mode, this frequency is much higher than those calculated or measured at 182.5 cm^{-1} (calculated values range from 178.3 to 221.9 cm^{-1}) and 158 cm^{-1} (calculated values range from 140.3 to 181.1 cm^{-1}) respectively for FeSe[54] and $Fe_{1.074}Te$[55]. Concerning the second E_g mode, the radial translation is in-phase leading to a breathing mode calculated at 396 cm^{-1} and could be matched with the experimental value was measured 402 cm^{-1}. This mode was found dependent of the spin phonon coupling for FeSe[54]. Indeed, including or not a on-site correlation parameter U equal to 5 eV, Kumar et al.[53] noticed a variation of 50 and 42 cm^{-1} for the two E_g modes evaluated on a non-magnetic model. However, based on the conclusion of Devey et al.[51] this shift linked to the Hubbard parameter could be non physic.

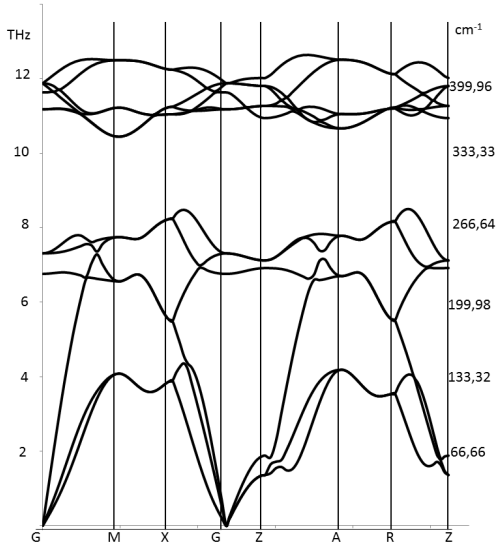

Fig. 3 The calculated phonon dispersion curves for the FeS structure given in directions defined by high symmetry point of the Brillouin zone.

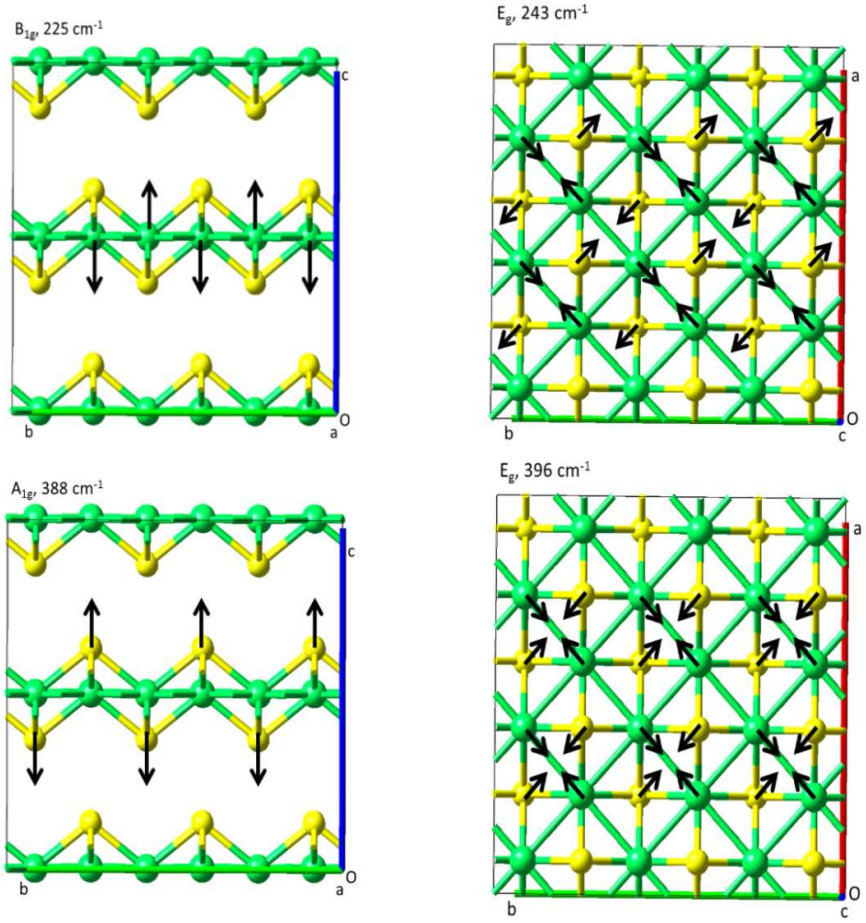

Fig. 4 Normal modes of mackinawite.

4. Conclusion

The mode frequencies and corresponding Raman vibrational assignments of mackinawite have been completed with a good accuracy. Theoretical results are successfully compared with our experimental data. On the experimental point of view, this result is a complete and more accurate interpretation of the mackinawite Raman spectrum, what was lacking in the literature. A precise characterisation of mackinawite is of high importance since mackinawite could be indicative of biogeochemical conditions (alkaline conditions, low sulfide concentrations, presence of sulphate reducing bacteria…). Different results based on DFT calculations exist in the literature for the FeX(X= Se, Te) series. However, the results are parameters dependent and a systematic study should be performed to assess the influence of the different parameters such as, magnetism, functional and Hubbard or Grimme corrections.

References

1 H. T. Jr. Evans, R. A. Berner, C. Milton, Valleriite and mackinawite. *Geol. Soc. America Program 1962, Annual Meeting,* 47a.
2 H. T. Jr. Evans, C. Milton, E. C. T. Chao, I. Adler, C. Mead, B. Ingram, R. A. Berner, *USGS Professional Papers*, 1964, **475-D**, 64.
3 I. B. Butler, D. Rickard, *Geochim. Cosmochim. Acta*., 2000, **64 (15)**, 2665.
4 R. E. Sweeney, I. R. Kaplan, *Econ. Geol*., 1973, **68 (5)**, 618.
5 Y. El Mendili, A. Abdelouas and J.-F. Bardeau, *RSC. Adv*., 2013, **3**, 15148.
6 R. A. Berner, *Am. J. Sci*., 1970, **268(1)**, 1.
7 M. J. Russell, A. J. Hall, *J. Geog. Soc. Lond*., 1997, **154**, 377.
8 J. H. P. Watson, B. A. Cressey, A. P. Roberts, D.C. Ellwood, J. M. Charnock, A. K. Soper, *J. Magn. Magn. Mater.*, 2000, **214**, 13.
9 R. Jeffrey, Corrosion of mild steel in coastal waters. Doctorate of Philosophy, University of Newcastle, NSW, Australia, 2003.
10 H.A. Videla, L.K. Herrera*, Int. Microbiol*., 2005, **8**, 169.
11 I.B. Beech, S.A. Campbell, F.C. Walsh, Microbial aspects of the low water on the corrosion of carbon steel, in: Proceedings of the 12th International Corrosion Congress, vol. 5B, Houston TX, NACE, 1993.
12 Y. El Mendili, A. Abdelouas and J.-F. Bardeau, *Phys. Chem. Chem. Phys*., 2013, **15**, 9197.
13 T. Kakegawa, H. Kawai, H. Ohmoto, *Geochim. Cosmochim. Acta.*, 1998, **62**, 3205.
14 J.H.P. Watson, D.C. Ellwood, Q. Deng, S. Mikhalowsky, C.E. Hayter, J. Evans, *Minerals Engineering*., 1995, **8**, 1097.
15 J. Holmes, *Appl. Geochem*., 1999, **14**, 277.
16 M. Mullet, S. Boursiquot, J.-J. Ehrhardt, *Colloids. Surf*., 2004, **244**, 77.
17 F.R. Livens, M.J. Jones, A.J. Hynes, J.M. Charnock, J.F.W. Mosselmans, C. Hennig, H. Steele, D. Collison, D.J. Vaughan, R.A.D. Pattrick, W.A. Reed, L.N. Moyes, *J. Environ. Radioactivity*., 2004, **74**, 211.
18 H.-C. Flemming, A. Leis, Sorption Properties of Biofilms. Encyclopedia of Environmental Microbiology. 2003
19 J.W. Morse, T. Arakaki, *Geochim. Cosmochim. Acta.*, 1993, **57**, 3635.

20 T.J. Gallegos, Y.-S. Han, K.F. Hayes, *Environ. Sci. Technol*., 2008, **42**, 9338.
21 R. R. Patterson, S. Fendorf, M. Fendorf, *Environ. Sci. Technol*., 1997, **31 (7)**, 2039.
22 A. C. Scheinost, L. Charlet, *Environ. Sci. Technol*., 2008, **42 (6)**, 1984.
23 J. Liu, Kalliat T. Valsaraj, and R.D. Delaune, *Environ. Eng. Sci*., 2009, **26**, 833.
24 E. D. Burton, R.T. Bush, L.A. Sullivan, R.K. Hocking, D.R.G. Mitchell, S.G. Johnston, R.W. Fitzpatrick, M. Raven, S. McClure, L. Y. Jang, *Environ. Sci. Technol*., 2009, **43**, 3128.
25 J. Liu, K.T. Valsaraj, I. Devai, R.D. DeLaune. *J. Hazard. Mater*., 2008,**157**, 432.
26 M. Wolthers, L. Charlet, P. R. van Der Linde, D. Rickard and C. H. van Der Weijden, *Geochim. Cosmochim. Acta.*, 2005, **69** (14), 3469.
27 J.A. Bourdoiseau, M. Jeannin, R. Sabot, C. Rémazeilles, P. Refait, *Corros. Sci*., 2008, 50, 3247.
28 S. Pineau, R. Sabot, L. Quillet, M. Jeannin, Ch. Caplat, I. Dupont-Morral ,Ph. Refait, *Corros. Sci*., 2008, **50**, 1099.
29 Y. El Mendili, A. Abdelouas and J.-F. Bardeau, *J. Mater. Environ. Sci*., 2013, **4**, 786.
30 J.A. Bourdoiseau, M. Jeannin, C. Remazeilles, R. Sabota, P. Refait, *J. Raman. Spectrosc*., 2011, **42**, 496.
31 M. Langumier, R. Sabot, R. Obame-Ndong, M. Jeannin, S. Sablé, Ph. Refait, *Corros. Sci*., 2009, **51**, 2694.
32 C. Rémazeilles, D. Neff, F. Kergourlay, E. Foy, E. Conforto, E. Guilminot, S. Reguer, Ph. Refait, Ph. Dillmann, *Corros. Sci*., 2009, **51**, 2932.
33 B.W.A. Sherar, I.M. Power, P.G. Keech, S. Mitlin, G. Southam, D.W. Shoesmith, *Corros. Sci*., 2011, 53, 955.
34 B.W.A. Sherar, P.G. Keech, D.W. Shoesmith, *Corros. Sci*., 2011, **53**, 3636.
35 B.W.A. Sherar, P.G. Keech, D.W. Shoesmith, *Corros. Sci*., 2013, **66**, 256.
36 R. A. Berner, *Science*, 1962, **137**, 669.
37 R. A. Berner, *J. Geol*., 1964, **72**, 293.
38 A.R. Lennie, S.A.T. Redfern, P.F. Schofield, D.J. Vaughan*, Mineral. Magazine*., 1995, **59**, 677.
39 M. Mullet, S. Boursiquot, M. Abdelmoula, J.-M. Génin, J.-J. Ehrhardt, *Geochim. Cosmochim. Acta.,* 2002, **66**, 829.
40 F.M. Michel, S.M. Antao, P.J. Chupas, P.L. Lee, J.B. Parise, M.A.A. Schoonen, *Chem. Mater*., 2005, **17**, 6246.
41 L.G. Benning, R.T. Wilkin, H.L. Barnes, *Chem. Geol*., 2000, **167**, 25.
42 M. Wolthers, S. Van der Gaast, D. Rickard, *Am. Mineral*., 2003, **88**, 2007.
43 X. Shi, K. Sun, L.P. Balogh, J.B. Baker Jr., *Nanotechnology*., 2006, **17**, 4554.
44 D. Renock, T. Gallegos, S. Utsunomiya, K. Hayes, R.C. Ewing, U. Becker, *Chem. Geol*., 2009, **268**, 116.
45 Y. El Mendili, A. Abdelouas and J.-F. Bardeau, *J. Mater. Eng. Perfor.*, 2014, **23(4)**,1350.
46 E. B. Hansson, M. S. Odziemkowski, R. W. Gillham, *Corros. Sci.,* 2006, **48**, 3767.
47 A. Wang, B.L. Jolliff, L.A. Haskin, *J. Geophys. Research*., 1995, **100**, 21189.
48 A. Jolivet, J.-F. Bardeau, R. Fablet, Y.M. Paulet H. de Pontual, *Anal. Bioanal. Chem* 2008, **392**, 551.
49 Sheri N. White, *Chem. Geol*., 2009, **259**, 240.
50 W. B. White. *Int. J. Speleology*., 2006, **35 (2)**, 103.
51 A.J. Devey, R. Grau-Crespo and N.H. de Leeuw, *J. Phys. Chem. C*., 2008, **112**, 10960.
52 K.D. Kwon, K. Refson, S. Bone, R. Qiao, W.L. Yag, Z. Liu, G. Sposito, *Phys. Rev. B*., 2011, **83**, 064402.
53 A. Kumar, P. Kumar, U.V. Wagmare, A.K. Sood, *J. Phys.: Condens. Matter*., 2010, **22**, 385701.

54 V. Gnezdilov, Y.G. Pashkevich, P. Lemmens, D. Wulferding, T. Shevtsova, A. Gusev, D. Chareev, A. Vasiliev, *Phys. Rev. B*., 2013, **87**, 144508.
55 T.L. Xia, D. Hou, S.C. Zhao, A.M. Zhang, G.F. Chen, J.L. Luo, N.L. Wang, J.H. Wei, Z.Y. Lu, Q.M. Zhang, *Phys. Rev. B.*, 2009, **79**, 140510.
56 K. Okazaki, S. Sugai, S. Niitaka and H. Takagi, *Phys. Rev. B*., **83** 035103, (2011)
57 ASTM Standards. Coupon test method D 2328-65 T. ASTM international standards worldwide. 1966.
58 Y. El Mendili, J.-F. Bardeau, N. Randrianantoandro, F. Grasset, J.-M. Grenèche, *J. Phys. Chem. C*. 2012, **116**, 23785.
59 Y. El Mendili, J.-F. Bardeau, N. Randrianantoandro, A. Gourbil, J.-M. Grenèche, A.-M. Mercier and F. Grasset, *J. Raman. Spectrosc*., 2011, **42**, 239.
60 Hoon Y. Jeong, Jun H. Lee, and Kim F. Hayes**,** *Geochim. Cosmochim. Acta*., 2008, **72(2)** 493.
61 A. R. Lennie, S. A. T. Redfern, P. E. Champness, C. P. Stoddart, P. F. Schofield, D. J. Vaughan, *Am. Mineralogist.*, 1997, **82**, 302.
62 A. Boughriet, R.S. Figueiredo, J. Laureyns, P. Recourt, *J. Chem. Soc*., *Faraday Trans.* 1997, **93**, 3209.
63 D. Rickard, *Stockholm Contrib. Geol.* 1969, **26**, 67.
64 A. R. Lennie and D. J. Vaughan, *Min. Spectr.*, 1996, **5**, 117.
65 H. Ohfuji, D. Rickard, *Earth Planet. Sci. Lett.*, 2006, **241**, 227.
66 D. J. Vaughan, A. R. Lennie, *Sci. Progr. Edinburgh.*, 1991, **75**, 371.
67 M. Farina, D.M. S. Esquivel, H. G. P. Lins de Barros, *Nature*., 1990, **343**, 256.
68 S. Mann, N. H. C. Sparks, R. B. Frankel,D. A. Bazylinski, H. W. Jannash, *Nature*., 1990, **343**, 258.
69 S. Boursiquot, M. Mullet, M. Abdelmoula, J.-M. Génin, J.-J. Ehrhardt, *Phys. Chem. Miner.*, 2001, **28**, 600.
70 D. Csákberényi-Malasics, M. Pósfai, J.D. Rodriguez-Blanco, L.G. Benning, V.K. Kis, A. Recnik, *Chem. Geol.*, 2012, **294-295**, 249.
71 G. Kresse and J. Furthmuller, *Phys. Rev. B*., 1996, **54**, 11169.
72 X. Chen, X. Zhang, J. Wan, Z. Wang, Y. Qian, Chem. Phys. Lett.2005, **403**, 396.
73 Materials Design Angel Fre NM
74 A. D. Becke, *Phys. Rev*., 1988, **38**, 3098.
75 C. Lee, W. Yang, R. G. Parr, *Phys. Rev. B.,* 1988, **37**, 785.
76 S. Grimme, *J. Comp. Chem*., 2006, **27**, 1787.
77 H.J. Monkhorst, J.D. Pack, *Phys. Rev. B*., 1976, **13**, 5188
78 K. Parlinski, Z.Q. Li and Y. Kawazoe, *Phys. Rev. Lett*., 1997, **78**, 4063.
79 E. Kroumova, M.I. Aroyo, J.M. Perez Mato, A. Kirov, C. Capillas, S. Ivantchev & H. Wondratschek, *Phase Transitions,* 2003, **76**, 155
80 M. I. Aroyo, D. Orobengoa, G. de la Flor, J. M. Perez-Mato and H. Wondratschek. *Acta Cryst.* 2014, **A70**, 126